JOURNAL OF PETROLEUM GEOMECHANICS
(JPG)

Original article

Non-Coaxial Multi-laminate model for anisotropic granular material and its numerical implementation

Shahrooz Shakeri[1*], Hasan Ghasemzadeh[2]

1- Ph.D., Civil Engineering Faculty, K. N. Toosi University of Technology, Tehran, Iran
2- Associate professor, Civil Engineering Faculty, K. N. Toosi University of Technology, Tehran, Iran

Received: 17 August 2023; Accepted: 15 October 2023

DOI: 10.22107/JPG.2023.409837.1206

Keywords

Fabric Assessment,
Damage,
Anisotropy,
Geo-Materials,
Multi-Laminate,
Stress Rotation

Abstract

Non-coaxiality plays a key role in modelling of problems with significant stress rotation in soil mechanics. This will be more crucial in types of soils or granular materials with anisotropy. Many of the constituent rocks of oil and gas reservoirs are of the anisotropic type, so considering anisotropy in the study of oil reservoirs will have special significance. Neglecting to account for stress and strain non-coaxiality would result in errors and overestimating soil capacity. A mathematical solution is developed and applied within the framework of multi-laminate model, to deal with this issue. Selecting multi-laminate frame as the base of the model facilitates consideration of anisotropy with less mathematical effort. In addition, tracing fabric evolution may be much easier in this framework. Concept of stress and strain vector fields are introduced for shear components of planes, and in contrast to ancestor multi-laminate models, shear stress is calculated through this concept for each plane in the proposed model. Using this method, non-coaxiality may be considered on planes, and consequently the integrated result of plane stresses will be non-coaxial as well. Finally, to apply the model for greater problems, a code is developed to introduce the new model to FE program, Opensees. The program is implemented for analyzing an experimental plane-strain loading test of an anisotropic dense specimen of Toyoura sand. The results show a good agreement between theory and experiment.

1. Introduction

Rocks and soils in nature are often anisotropic. In various industries that deal with the natural materials of rocks and soils, having an anisotropic mechanical behavior model is always necessary. For example, in drilling oil and gas reservoirs, considering an appropriate mechanical model to predict the behavior of anisotropic rocks can greatly assist in proper wellbore design. Additionally, in enhanced oil recovery methods that require hydraulic fracturing of wellbores, predicting the direction of created fractures necessitates knowledge of the mechanical behavior of anisotropic rocks. In mining operations, finding the optimal mining path, which is shorter and safer, requires knowledge of the appropriate mechanical behavior model for anisotropic rocks. In other industries, such as tunneling and deep-water well drilling, similar conditions prevail as well. The surrounding environment, which can consist of rock, soil, or a combination of them, has constantly been subjected to various stresses such as tectonic stress, overburden stress, thermal stress, or even fluid pressure throughout the years. As a result, the structure of these environments often changes to anisotropic state over long periods, making the prediction of their mechanical behavior challenging. For example, in the upstream oil and gas industry, successful application of advanced methods such as hydraulic fracturing in different fields relies on employing suitable models to predict the mechanical behavior of the reservoir rock [1]. If the behavior model used in hydraulic

* **Corresponding Author:** shahrooz.shakeri@gmail.com

fracturing studies cannot consider the anisotropic properties of the reservoir rock and the variable nature of applied stresses, finding the optimal location for hydraulic fracturing and creating fractures in the desired direction becomes difficult or leads to operational challenges. In such cases, besides anisotropy, the non-coaxiality of principal stresses at various points in the surrounding environment and their rotational directions can also influence the behavior of rocks or soil. Most of the problems in geotechnical engineering, encounter with variable stress paths. Direction of principal axes of stress tensor is not kept constant in real problems. Applied stresses in a problem may change in magnitude and direction simultaneously during loading process. Both of these factors have a significant impact on instant and permanent deformation of granular material. Experimental evidences show that, even with constant magnitudes of principal stresses, rotation of principal axes changes the fabric of grains, and cause some displacements and deformations in the texture of the material [2]. Yang and Yu [3] compared the results of coaxial and non-coaxial models for foundation settlements and soil bearing capacity under different loading and boundary conditions. They found that settlement of a footing is much more when non-coaxiality between stress and strain rate is taken into account. Discrepancies between the results of the two models significantly increase with increasing rotation of principal axes of stress. Therefore, lack of attention to non-coaxiality may lead to non-conservative design of foundations [3]. Gräbe and Clayton [4] investigated soil foundation of rail tracks. They showed that a real evaluation of total life cost of such foundations directly depends on the repeated principal stress rotation applied by trains. In addition, they explained in detail, the importance of considering principal stress rotation in evaluating permanent displacements of soil foundations of rail tracks. The importance of use of more appropriate testing methods such as the cyclic simple shear apparatus or the cyclic hollow cylinder is highlighted in the above mentiond study as well. Other experimental observations also indicate that a significant plastic deformation happens during principal stress rotation, while the magnitudes of principal stresses are kept constant. Hollow cylinder test results suggest that volumetric strain during rotational shear tests is usually contractive, and the soil sample approaches a stable state after a couple of cycles [5]. These results also indicate the non-coaxiality between stress and strain, and show that the non-coaxiality significantly depends on the stress ratio.

While principal axes of stress tensor rotate, strain tensor axes rotate simultaneously, with a different rate, resulting in non-coaxiality. As just described above, the importance of non-coaxiality is clear enough. It has been one of the major concerns of the geotechnical engineers for decades. Due to the dependency of conventional models to stress tensor invariants, they are not capable to consider principal axes rotation. In such models, it is assumed that coaxiality exists between the directions of principal stresses and plastic strain increments. Therefore, it limits the application of these models only to cases in which stress axes do not rotate [6]. In order to come up with this issue, researchers have proposed some solutions through applying modifications to the existing models. According to some specifications of multi-laminate models, they are among the first choices to account for principal axes rotation. Based on the multi-laminate model, Bažant and Oh [7] developed a new method to calculate the behavior of brittle geomaterials which experience progressive tensile fracturing or damage. The response of the proposed model was path dependent. Using multi-laminate as the foundation of model allows to apply rotation of principal axes to the problems with progressive fracturing, and hence, tensorial invariance restrictions are captured by the multi-laminate outline.

Borja *et al.*, [8], utilizing a numerical algorithm for tensor invariants, developed a new plastic isotropically hardening model. They were irrespective of the anisotropy characteristics of the materials, which might affect the results. Li and Dafalias [9] studied anisotropic materials in a research program. In this study, they used a modified form of critical state soil mechanics, to describe a plasticity constitutive model for inherent anisotropic sand behavior. Fabric of the inherent anisotropic material is mathematically presented by a second-order symmetric fabric tensor, Fij, in this model. A scalar-valued parameter "A" is introduced to the model, to calculate anisotropy effects. This parameter is defined in terms of invariants of fabric and stress tensor. The variation of the critical state line geometry in the plane of void ratio and effective mean normal stress is determined by "A". In other

words, all other soil mechanical parameters will be a function of "A" , as well. In a similar study, Gao *et al.* [10] developed another failure criterion for geomaterials. This model is capable to take into account the effect of cross-anisotropy. The failure criterion depends on the frictional coefficient, and it varies in different directions by changing this coefficient. Frictional coefficient in this model is defined as a function of an anisotropic variable such as the previously mentioned A.

The impact of inherent and induced anisotropy, and variation of material fabric in different steps of loading, has never been the study subject of any of the above models. In spite of the very few theoretical studies in this regard, a considerable number of experimental studies on rotation and non-coaxiality between stress and strain has been implemented. Miura et al. [2] have done a lot of research on sand behavior and deformation under the impact of cyclic and rotational loading. Also, a series of drained tests on anisotropic dense sand, using hollow cylinder, have been done by other researchers. They showed that shear deformation under rotational stress loading is greater, compared to fixed axis stress [2,11,12,13,14]. Moreover, these studies have proven that the impact of inherent anisotropy of material on shear deformation and volumetric variations of the sample, with rotational and cyclic loading, is more than that on fixed axes mode. Thus, the importance and necessity of simultaneously considering anisotropy and the impact of stress axes rotation can be seen more than ever. Other researchers also studied behavior of different sands in rotational and cyclic loadings, using hollow cylinder. All the results proved non-coaxiality between stress and strain and the necessity of considering the anisotropy of material during the rotation of principal stress axes [11, 12, 15, 16, 17].

In this study, in addition to the modification of multi-laminate models, a new method for considering the rotation of stress or strain axes and involving non-coaxiality in anisotropic materials have been presented. Upon explaining the method and presenting computational relations, a practical code is developed to introduce the proposed method to finite element program Opensees, and its application in problem solving is shown. The case under study in this research is the process of shear band formation in a sample of standard Toyoura sand, in which the variations of particles arrangement, deformations and strength of the sample are studied and investigated and compared with the theoretical results obtained from the Opensees program in assistance with the above-mentioned code.

2. Formulas and Frameworks of Multi-laminate Models

In classic continuum models, stress or strain tensor components are defined on a cubic surface. In these models, an infinitesimal cube, with dimensions dx , dy and dz , defined around a point, which is only capable to define those components of stress or strain tensor which are either laid on or perpendicular to one of these surfaces. This brings up some constraints. Considering only six orthogonal planes from among the infinite planes around a point may cause deletion of the events that might occur on other planes, and affect the material behavior. Nonlinear behaviors of the materials are highly influenced by stress and strain path and its history. So, by deletion of the impact of other planes, prediction of results by the model, especially regarding the anisotropic materials, may not be precise enough. Ignoring the effect of different directions around a point in anisotropic materials certainly has so many negative impacts on the model result accuracy.

In order to consider and aggregate the infinite effects of planes around a point, instead of studying a cubic surface, a spherical surface should be studied. Any point on a spherical surface represents the tangential plane on that point of the sphere, and displays the effects of that specific plane. In order to measure the stress components at a point, the stress should be integrated on the surface of the circumferential sphere. Numerical methods may be used for calculating this integral. To simplify the issue, the integrand function on specific points of the sphere is measured, multiplied by the relevant weight factors, and eventually their sum will be calculated as the numerical integral over the spherical surface. In fact, using this method, the spherical surface is estimated by a geometrical polyhedron. It is obvious that by increasing the number of sides of the polyhedron, accuracy of results will be increased. A comprehensive mathematical discussion regarding the number of planes used in this estimation, the method of computing weight factors and the expected value

of error is suggested in Ref. [18].

Ideally, in granular materials like sand, their response to the applied loads could be calculated using micro-mechanical behavior. In fact, material behavior is mostly influenced by the movement of constituent grains, including sliding and rolling. For this, environmental stress distribution, characteristics of fabric, kinematic characteristics of the grains (sliding, rolling or both), and kinematic constitutive laws of the grains should be clear. In this regard in each step of loading, by doing calculations, the new condition of all factors, parameters and fabric of the grains to be obtained, and the basis for further computations to be brought about. Representing the macro-level stress tensor of each point in terms of micro-level stresses, the number and value of contact forces and the contact conditions of micro-level points have long been the goal of many researchers [19, 20].

Multi-laminate models are, to a great extent, the answer to the above need. These models, defining the interconnected particles as the material particles and grains, are considerably capable to pave the way for the simulation of micro-level forces among the grains. According to the assumptions of this method, considering slide or separation among the grains will be possible. The forces applied to different sides of the polyhedron are expressive of the same forces applied to the interconnected elements of material.

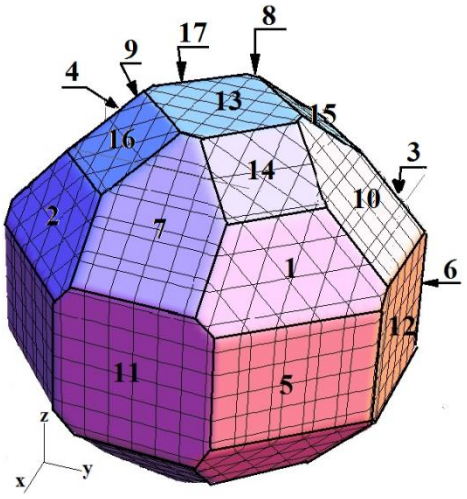

Fig. 1. Location of Different planes in the given 34-plane Polyhedron

Fig. 1 shows the arrangement of planes and different sides of a polyhedron that approximates the spherical surface around a point. This polyhedron includes 2x17 sampling planes. The directions of normal vectors of all planes are shown in Table 1 [21, 22]. In some of the multi-laminate models, a polyhedron with 2x13 planes, was used, in which there were incompatibility between stress and strain tensors, and are explained in detail, in Refs. [22, 23]. Therefore, in this study, 34 planes are used, which increase the precision of computations, as well as solving the problem of inconsistency between stress and strain of local and global coordination systems. Considering the symmetry of the polyhedral geometry, directions of normal vectors of only half of its planes and related weight factors are presented in Table 1. Orientation of other planes, considering their symmetry, is computable.

Table 1. Direction Cosines and Weight Factors of Different Planes in the 34-plane Polyhedron [21, 22]

Plane No.	Direction Cosine with respect to x axis	Direction Cosine with respect to y axis	Direction Cosine with respect to z axis	Weight Factor
1	$1/\sqrt{3}$	$1/\sqrt{3}$	$1/\sqrt{3}$	0.020277985
2	$-1/\sqrt{3}$	$1/\sqrt{3}$	$1/\sqrt{3}$	0.020277985
3	$1/\sqrt{3}$	$-1/\sqrt{3}$	$1/\sqrt{3}$	0.020277985
4	$-1/\sqrt{3}$	$-1/\sqrt{3}$	$1/\sqrt{3}$	0.020277985
5	$1/\sqrt{2}$	$1/\sqrt{2}$	0	0.058130468
6	$-1/\sqrt{2}$	$1/\sqrt{2}$	0	0.058130468
7	0	$1/\sqrt{2}$	$1/\sqrt{2}$	0.030091134
8	0	$-1/\sqrt{2}$	$1/\sqrt{2}$	0.030091134
9	$-1/\sqrt{2}$	0	$1/\sqrt{2}$	0.030091134
10	$1/\sqrt{2}$	0	$1/\sqrt{2}$	0.030091134
11	1	0	0	0.038296881
12	0	1	0	0.038296881
13	0	0	1	0.02930060
14	$-1/\sqrt{6}$	$-1/\sqrt{6}$	$\sqrt{2/3}$	0.019070616
15	$1/\sqrt{6}$	$-1/\sqrt{6}$	$\sqrt{2/3}$	0.019070616
16	$-1/\sqrt{6}$	$1/\sqrt{6}$	$\sqrt{2/3}$	0.019070616
17	$1/\sqrt{6}$	$1/\sqrt{6}$	$\sqrt{2/3}$	0.019070616

To evaluate a function value at each point, given the function values on different planes of the polyhedron, the following well known relation can be used:

$$\iint_{\Omega} f(x,y,z) = 4\pi \sum_{i=1}^{17} w_i f(x_i, y_i, z_i) \qquad (1)$$

where Ω presents the unity sphere surface, $f(x,y,z)$ shows the arbitrary function on the

unity sphere surface, and w_i is the weight factor of the i th plane.

As mentioned previously, in classic continuum models, constitutive relations are written between macroscopic stress and strain invariants, and values of stress and strain tensor components are directly related to each other. In multi-laminate models, constitutive relations between stress and strain already exist, but these relations are written in micro-level scale and between the stress and strain of planes. In each step of loading, the strains of the planes are the projection of macro-level strain tensor. Considering this kinematic constraint, the consistency of strains between micro and macro level are guaranteed. In addition, static equilibrium of the model is enforced by applying the principle of virtual work during loading process even after the maximum stress point and at the strain softening area [24].

An optional plane, and projected vectors of macro-level strain, is shown in Fig. 2. In this Fig., "N" is normal vector of the sample plane, and "M" and "L", which can be desirably selected, are the tangential vectors of planes. This orthogonal system of vectors forms a local coordinate system. In this study, to facilitate the computations and without any reduction in the generality of the matter, all the "M" vectors in different planes are considered to be perpendicular to the global direction "Z".

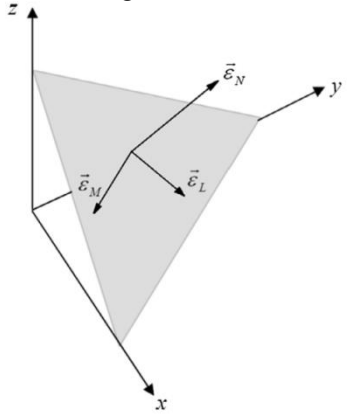

Fig. 2. An arbitrary Sample plane and its related Normal and Shear vectors of Strain

Due to the kinematic constraint, which is assumed for developing the model, normal and shear strain in different planes can be calculated using tensor transformation equations:

$$\varepsilon_N = n_i \varepsilon_{ij} n_j \quad , \quad \varepsilon_M = m_i \varepsilon_{ij} n_j \quad , \quad \varepsilon_L = l_i \varepsilon_{ij} n_j \qquad (2)$$

In this equation, ε_{ij} is strain tensor component, l_i, m_i and n_i are the direction cosines of L, M and N vectors, respectively. Also, according to Fig. 2, the projected vectors of strain tensor on an arbitrary plane in normal and shear directions are shown with ε_N, ε_M and ε_L. Repetition of subscripts in Eq. 2 represents the sum of mathematical terms for $i = 1,2,3$.

In the orthogonal local coordination system, relation $\vec{n} = \vec{m} \times \vec{l}$ exists among the vectors. N_{ij}, M_{ij}, L_{ij} tensors could be defined as follows:

$$\begin{aligned} N_{ij} &= n_i n_j \\ M_{ij} &= \frac{m_i n_j + m_j n_i}{2} \\ L_{ij} &= (l_i n_j + l_j n_i)/2 \end{aligned} \qquad (3)$$

According to this equation, strain vectors in different planes may be written as follows:

$$\varepsilon_N = N_{ij}\, \varepsilon_{ij} \quad , \quad \varepsilon_M = M_{ij}\, \varepsilon_{ij} \quad , \quad \varepsilon_L = L_{ij}\, \varepsilon_{ij} \qquad (4)$$

Virtual work equation between macro-level (inside the unity sphere) and micro-level (on the spherical surface) scales may be written and following equation will be obtained [24]:

$$\sigma_{ij} = \frac{3}{2\pi} \int_{\Omega} \left[\sigma_N\, N_{ij} + \sigma_M\, M_{ij} + \sigma_L\, L_{ij} \right] d\Omega \qquad (5)$$

In Eq. 5, σ_N is the normal stress vector and σ_M, σ_L are the shear stress vectors of the desirable plane. Using Eq. 5, in each load increment, the components of macro-level stress tensor σ_{ij} can be calculated based on the stress vectors of planes.

It can be proved that, in elastic state, the relation between stress and strain on the planes may be written as follows [24, 25]:

$$\sigma_N = E_N . \varepsilon_N \quad , \quad \sigma_M = E_T . \varepsilon_M \quad , \quad \sigma_L = E_T . \varepsilon_L \qquad (6)$$

where E_N, E_T are normal and shear elastic moduli of the planes, and their relation with elastic modulus, E, and Poisson ratio υ is shown in Refs. [24, 25]:

$$E_N = E/(1-2\upsilon) \quad , \quad E_T = E(1-4\upsilon)/((1+\upsilon)(1-2\upsilon)) \qquad (7)$$

To compute the components of macro-level stress tensor, due to Eq. (5), the relevant integral should be computed on the spherical surface Ω. This integral may be computed in one of the approximate numerical methods, such as Gaussian Method. In this method, as mentioned previously, the weighted summation of a desirable function $f(n_1, n_2, n_3)$ on the planes is calculated. Same as numerical integration on a plane surface, in spherical integration also the value of function in each plane is computed and after multiplying it

by the relevant weight factor, summation of planes is found. The numerical integral of Eq. (5), which was resulted from the principal of virtual work, is as follows [24]:

$$\sigma_{ij} = \frac{3}{2\pi}\int_{\Omega} S_{ij}\, d\Omega \approx \frac{3}{2\pi} \times 4\pi \times \sum_{p=1}^{N_p=17} w_p (S_{ij})_{(p)} \qquad (8)$$
$$S_{ij} = \sigma_N N_{ij} + \sigma_M M_{ij} + \sigma_L L_{ij}$$

In this equation, p is the plane number and N_p is the total number of planes.

3. Review on Damage Theory and the Applied Relations

When strain components on the planes, i.e., $\varepsilon_N, \varepsilon_M, \varepsilon_L$ are calculated, for the very early steps of loading, the values of the continuum stress may be computed using Eq. (8). But gradually by the increase of the applied loads, development of micro cracks, and their interconnection, this relation loses its linear form, and hence the reduction of rigidity of material should be taken into account in calculating the stress. Some explanations on the reasons and factors of rigidity deterioration of different geo-materials have been provided formerly, and it has been repeatedly dealt with in literature and different articles [26, 27, 28]. To consider the degradation in the rigidity and strength of material and their nonlinear properties in the developed model, damage functions are used. The role of these functions is to control the decrease in normal and shear stiffness in different planes. These functions, in each step of loading, by increasing the strains, calculate the extent of damage imposed to the material, and modifies the stiffness values by applying a mathematical factor between 0 (intact case) and 1 (fully damaged). Damage functions are shown with ω and $(1-\omega)$ will be a factor which in each step modifies the value of the initial stiffness, and computes the value of the applicable stiffness factor.

Many different functions could be considered for ω, but depending on the conditions and characteristics of each type of material, they may be different in each model. In the current model, to reduce the number of parameters and for maintaining the necessary accuracy, exponential functions are used in general form $\omega = 1 - Exp(-(\varepsilon/a)^b)$. Decrease in the number of parameters lets one to find them more easily in calibration stage, and at the same time, simpler relations and eventually a sharper model to be obtained. For each given strain component in the model, (tensile, compressive or shear), two parameters will be needed, and added to the model.

Selecting different values for a and b, stress-strain relation curves could desirably been achieved. The main role of parameter b is to adjust the value of drop slope and the sharpness of the maximum point of stress-strain curve. Parameter a also determines the position of peak point of stress-strain curve.

In general, three types of the strains may be applied to a plane: tensile, compressive and shear. In geo-materials, three damage functions may be considered to calculate damages applied to the material appropriately.

Considering that the current study is dedicated to the behavior of anisotropic sands, tensile strength of material is ignored for simplicity and only compressive and shear strength are taken into account in computations. According to the presented explanations, two series of parameters a and b are considered for sands, in model: a_{Nc}, b_{Nc} for the normal compressive damage function and a_T, b_T for the shear damage function of the planes. Hence the stresses on different planes are extracted from the following relations:

$$\sigma_N = 0 \quad ; \quad \varepsilon_N > 0$$
$$\sigma_N = (1-\omega_{Nc}).E_N^0.\varepsilon_N \quad ; \quad \varepsilon_N \le 0 \qquad (9)$$
$$\sigma_T = 0 \quad ; \quad \varepsilon_N > 0$$
$$\sigma_T = RF_T.(1-\omega_T).E_T^0.\varepsilon_T \quad ; \quad \varepsilon_N \le 0 \qquad (10)$$

$\varepsilon_N > 0$ is the equivalent for tensile strains and $\varepsilon_N < 0$ is the equivalent for compressive strains. In Eqs. (9) and (10), the values of compressive damage function and shear damage function are computed, respectively, as follows:

$$\omega_{Nc} = 1 - Exp(-(\varepsilon/a_{Nc})^{b_{Nc}}) \qquad (11)$$
$$\omega_T = 1 - Exp(-(\varepsilon/a_T)^{b_T}) \qquad (12)$$

It is assumed that if unloading and reloading occurs in the normal component of planes, damage factor would not change [29], and remain constant until normal strain reaches its maximum value in the strain history. The function diagram of damage factors, in this condition, act as an envelope for damage factors, and the maximum value of the strain is the return point of the damage factor to the envelope Fig. 3.

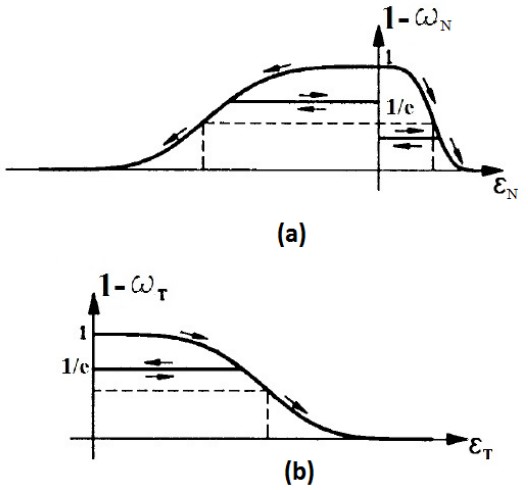

Fig. 3. Variations of the Damage Factor Values in Loading and Unloading [29]: (a) Damage Function of the normal Strains (b) Damage Function of the normal Strains

Using different planes in different directions enhance multi-laminate models with special properties. In this type of models, some of the planes enter into unloading stage, while other planes are still loading. This property can be seen in no other model, and compared to the classic continuum models, this is considered to be a privilege. The reason for this property is that stress and strain vectors on different planes are not tensor, thus do not need to fulfill any tonsorial invariance condition. Unloading in the model occurs when the value of the work performed, $\sigma.\Delta\varepsilon$, is negative. This criterion of unloading is considered independently for each stress component on different planes.

4. Inherent Anisotropy of Material

Anisotropy of material is categorized into two general types. Type 1 is the anisotropy which exists in the material from the very beginning, and is called inherent anisotropy. This type of anisotropy is resulted from the texture and microscopic constitution of materials and fabric of the grains. Distribution of contact points in different spatial directions around a particle which is influenced by the orientation of sedimentation or tectonic pressure is the main reason for this type of anisotropy.

The mechanical properties of anisotropic materials vary in different directions. This variation in material behavior in different directions stems from the fabric of grains around a point, which is changing continuously while loading. Defining a uniform law for the whole planes facilitates the process of building and developing a model. If a rule is set, which can be used in all the planes, dispersion of relations and formulas will be reduced, and thus finding and calibrating the parameters, used in the model, will be much easier. In this model, due to the requirements and applications, compressive strength and shear strength are defined through the definition of ellipsoids. An ellipse is defined by a few numbers of parameters, but provides the model with the ability and competence to present a comprehensive and general law for determining the strength of each plane in each direction, which needs the least mathematical computations. There is a detailed discussion on the reasons and factors of variations in compressive strength and shear strength of the anisotropic material in different directions, as well as the appropriate geometric form for regularizing strength variations on different planes are presented in Refs. [23, 30].

For taking these variations in strength magnitude of different planes into account, two separate ellipsoids, for computing normal and shear stresses of the planes, should be considered. In this regard, one ellipsoid for normal compressive rigidity factor of the planes and another ellipsoid for shear rigidity factor of the planes are considered to introduce inherent anisotropy. According to this method, the stresses on each plane are calculated similar to isotropic mode, but rigidity factors, which modify the mobilized strength of each plane, are multiplied by the computed stresses, and modified stresses in anisotropic case are calculated according to the following relation:

$$\sigma_{Nc} = RF_{Nc}.(1-\omega_{Nc}).E_N^0.\varepsilon_{Nc}^{(p)} \qquad (13)$$

In this relation, RF_{Nc} defines the rigidity factor of the normal compressive strength.

An ellipsoid of normal rigidity factor is shown in Fig. 4(a). By extending the normal vector of the given plane, the vector cuts off the ellipsoid surface at point "**M**". The size of radius "**OM**" determines the value of normal rigidity factor for this specific plane. It is obvious that for an isotropic material, the three main radii of this ellipsoid are the same and equal to unity.

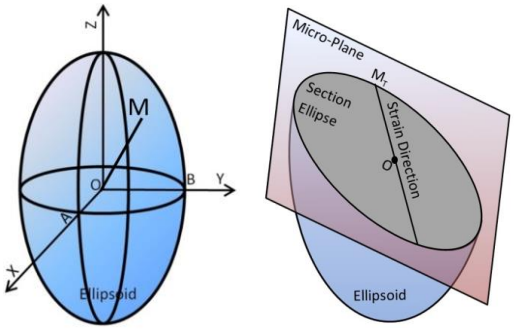

(a) **(b)**

Fig. 4. Ellipsoid of rigidity factors (a) Normal rigidity (b) Shear rigidity

Ellipsoid Equation for normal compressive rigidity factor is presented as follows:

$$\frac{l^2}{A_{Nc}^2}+\frac{m^2}{B_{Nc}^2}+\frac{n^2}{C_{Nc}^2}=1 \quad (14)$$

In Eq. 14, parameters A_{Nc}, B_{Nc}, C_{Nc} are the sizes of the main radii of these ellipsoids and are among the material constants, so should be found through calibration. The larger size of radius of the ellipsoid indicates larger strength of material on a specific direction.

Ellipsoid of material rigidity factors, for computing shear stresses, is shown in Fig. 4(b). This ellipsoid is cut by a given inclined plane which makes angles with all the three axes of the coordination system. If the value of shear strain on this plane equals ε_T , the value of the resultant shear stress on this plane will be σ_T , which is the product of shear strain and shear elastic modulus, E_T , and for this, vectors of stress and strain on the plane will be coaxial. The value of E_T depends on the direction of plane and the direction of shear strain itself. The more the plane conforms to the bedding plane, the less shear elastic modulus expected. In shear strains parallel to the direction of bedding plane, since it is easier for the grains to slide on each other, less energy is needed and less shear strength is created. The principal diameters of the ellipsoid are the rigidity factors of material in three directions, where eventually through multiplying them by E_T , shear elastic modulus in principal directions is obtained. In Fig. 4(b), "O" is the center of the ellipsoid and M_T is the point where strain vector of plane touches the surface of ellipsoid. By definition, the length of OM_T equals the value of rigidity factor in that direction. The value of shear stress on the planes, depending on normal strain mode, is also computed as follows:

$$\sigma_T = RF_T.(1-\omega_T^0).E_T^0.\varepsilon_T \ if \ \ \varepsilon_N \le 0 \quad (15)$$

$$\sigma_T = 0 \ \ if \ \ \varepsilon_N > 0 \quad (16)$$

It is obvious that for isotropic material, the principal diameters of the ellipsoid are all equal to one, and a sphere takes the place of the ellipsoid. The equation for ellipsoid is generally as follows:

$$\frac{l^2}{A_T^2}+\frac{m^2}{B_T^2}+\frac{n^2}{C_T^2}=1 \quad (17)$$

In this relation, A_T, B_T, C_T are the main radii of this ellipsoid, and are among the material constants, which should be found through calibration and comparison of the experimental and computational results.

Due to several experimental and laboratory observations, unloading and reloading of shear component cause some of the grains and particles of the sand, which were dispositioned and displaced during the initial loading, return back to their initial position, and the initial fabric of the grains to be regenerated and repaired to some extent. Recovery of sand texture during unloading and reverse loading results in an increase in density of texture and shear stiffness. This phenomenon is explained in different laboratory Refs. [31, 32], and makes the shear loading and unloading behavior of grain materials more complicated. In this study, considering the need, unloading and loading behavior of sand should be precisely computed in each step of loading, so that the maximum conformity with the experimental results to be obtained. To facilitate the computations, the issue is regularized by setting a series of simple rules to be introduced to the model, so that no new parameter to be added to the model, and thus calibrating results and finding parameters to be easier. The details of this method are explained in Ref. [23], so repetition is avoided.

5. Induced Anisotropy of Materials and Fabric Variations

The second type of anisotropy, is induced anisotropy. This type of anisotropy in materials occurs upon loading, and depends on the history and direction of loading. By loading progress and strains growth, the fabric and layout of grains will be changed. According to the experimental observations, variations of texture and material constitution always occur the way the direction perpendicular to the grains contact surface settles on the main direction of the maximum applied

compressive stress. In other words, the fabric of grains changes the way they can bear more load. For this, the neighboring grains move and displace the way they make column type strands along the principal compressive stress. Over time, the number of consistent grains in each strand and also the number of strands increase, and thus failure occurs. The above explanations are based on the experimental observations which are mentioned in different Refs. [33, 34]. At the moment of failure, the column type strands (load transfer paths) involve in buckling and failure one by one, and the material strength suddenly decreases in this direction.

Normal and shear stresses both change the fabric of grains, as well as the material particles. These variations in the fabric of grains and thus variations in the strength and rigidity of materials in different directions can be interpreted as variations of the ellipsoids of normal and shear strength. Variations of damage factors in different planes cause changes in size and dimensions of the ellipsoids in different directions. In fact, it can be said that these variations in the strength and rigidity of material in different directions are the result of variations of grains fabric. Planes with more loading and greater damage factors will decrease the dimensions of ellipsoid to a greater extent. Variations of the ellipsoids radii sizes in different directions result in the rotation of ellipsoids, and even change their geometrical shape to unusual ones. For example, in a uniaxial compressive loading which specimen subjects to lateral expansion, the maximum compressive strain is experienced on the planes perpendicular to the loading direction. The schematic diagrams of variations in the ellipsoid of the normal compressive rigidity factors are step by step presented in Fig. 5 (steps 1 to 5) in purple color (butterfly shape). The initial ellipsoid section is also shown by dashed line at the same part of the figure. Growth of normal strains distribution around a point (petal shape) in all steps is also, simultaneously, shown in blue in the figures. Vertical petals relate to the distribution of compressive strains and horizontal petals relate to the tensile strains. It is obvious from these figures that the increase in normal compressive strain is accompanied by an increase in horizontal tensile strain. In these steps of loading, the principal axes of the applied strain do not undergo any rotation, and remain fixed. As can be seen in these figures, the planes parallel to the loading direction, which have no compressive strain, are safe from the viewpoint of compressive damage, and no decrease in the diameter of ellipsoid can be seen on these planes. In other words, reviewing these ellipsoids, it can be said that those directions which have undergone greater decrease of dimension, are in fact more damaged. As loading proceeds, more planes undergo compressive damage and rigidity reduction. It is worth saying that distribution of strain and rigidity in this figure is in fact three dimensional, but to facilitate the display, in this figure, variations of strains and thus variations of ellipsoids are both shown in two dimensions. On the right side of the conceptual Fig. 5(steps 6 to 10), tensor axes start rotating by keeping the eigenvalues of the strain tensors constant. By the rotation of strain tensor axes, some of the planes are loaded and the values of their strain increase, but in contrast, some other planes are unloaded, which means the values of their strain decrease. As explained formerly, during the compressive unloading and by a decrease in the values of normal compressive strain, the factors of normal compressive damage do not decrease and remain constant. So those directions of the ellipsoid which are unloaded remain constant in size and do not change, but those directions which are being loaded become smaller in radius. In steps 6 to 10 of Fig. 5, it is observed that the diameter of the ellipsoids decreases gradually, which is indicative of the reduction in the compressive strength on that specific direction.

The way of considering the effect of shear strains of planes on the fabric of grains and particles is a little different. According to the relations of solid mechanics, it is clear that on each plane there is a direction on which the shear strain is higher than other directions. This direction is named the maximum shear strain direction of the plane. Also the direction perpendicular to the maximum shear strain of the plane lacks shear strain, and actually its shear strain is equal to zero. In each plane, it is expected that the maximum reduction in strength and shear

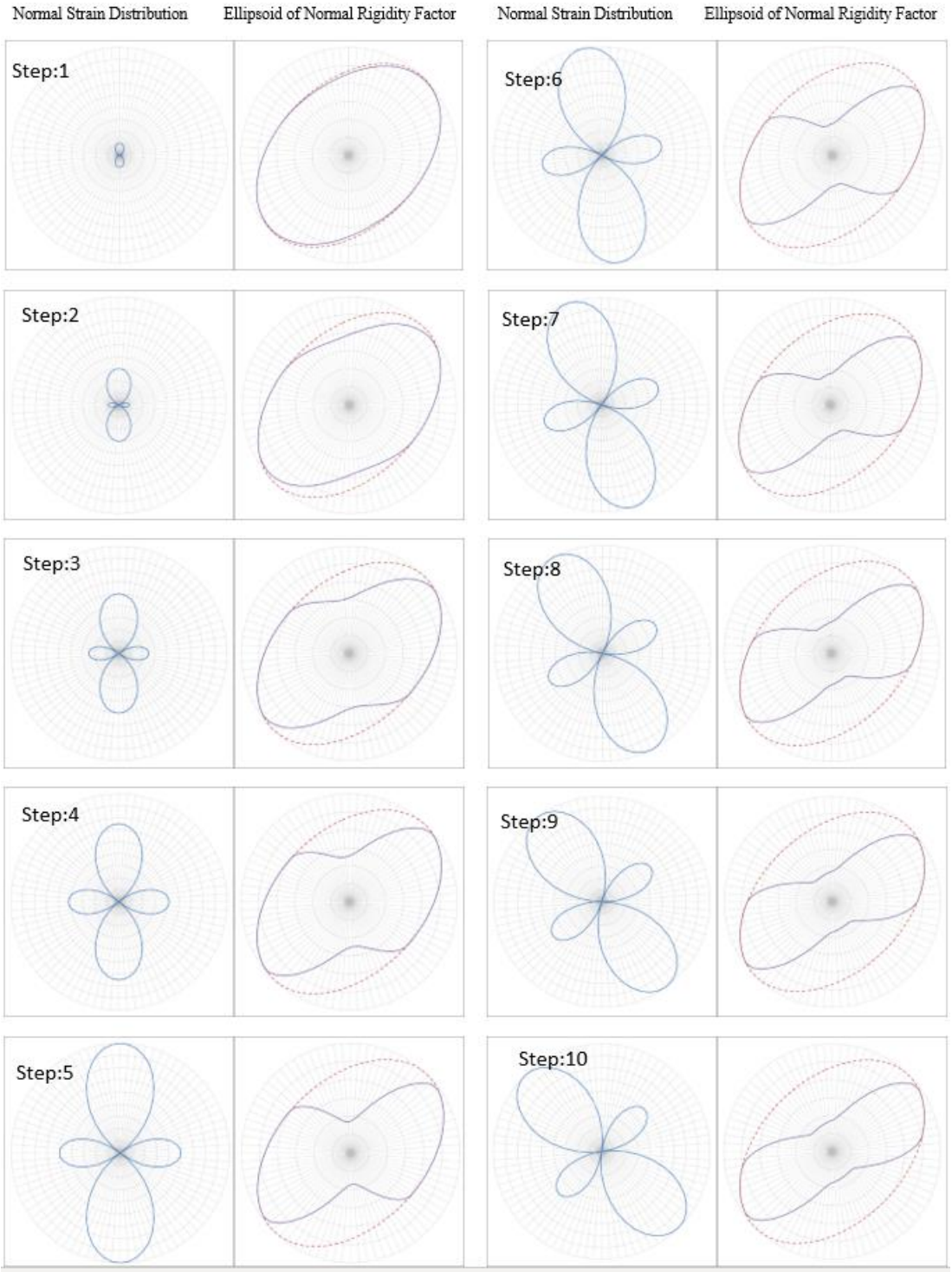

Fig. 5. Conceptual variations of strain distribution (blue petal) and the ellipsoid of normal Compressive rigidity factors (purple butterfly) – (steps 1-5: uniaxial Compressive loading, steps 6-10: rotation of principle axes)

rigidity of material to be along the maximum shear strain. Other directions on the plane are exposed to less shear stain and shear damage. So the direction perpendicular to the maximum shear

strain on each plane, the shear strain of which equals zero, will lack any shear damage and strength reduction [23,30].

The way of considering the effect of shear strains of planes on the fabric of grains and particles is a little different. According to the relations of solid mechanics, it is clear that on each plane there is a direction on which the shear strain is higher than other directions. This direction is named the maximum shear strain direction of the plane. Also, the direction perpendicular to the maximum shear strain of the plane lacks shear strain, and actually its shear strain is equal to zero. In each plane, it is expected that the maximum reduction in strength and shear rigidity of material to be along the maximum shear strain. Other directions on the plane are exposed to less shear stain and shear damage. So the direction perpendicular to the maximum shear strain on each plane, the shear strain of which equals zero, will lack any shear damage and strength reduction [23,30].

Each of the planes cut off the primary ellipsoid of the shear rigidity factor in an ellipse shape. All ellipses are produced from a mother ellipsoid. Each of the ellipses on the planes determines the process of variation of shear rigidity factors in different directions of that plane. When loading begins, shear strains of different planes start increasing.

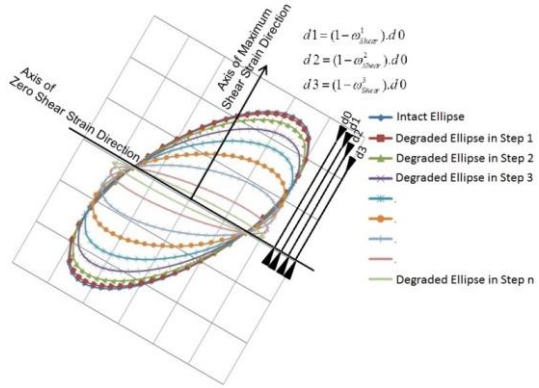

Fig. 6. Degradation and Rotation of principle axes of a sample shear rigidity factor on planes due to loading progress

Fig. 6 shows the conceptual process of rigidity factor degradation and also the rotation of the principle axes of a sample shear rigidity factor ellipse of a plane due to loading increase. As seen from the figure, the main axes of this ellipse are rotating on the plane while the strains are increasing and the stiffness is degrading. These variations in stiffness and rotation of axes are the result of fabric change. Knowing the mathematical equations of the ellipses in each step, shear rigidity factor of the plane in each direction will be computable through the equation of this ellipse, so the rotation of strain vector of each plane will impose no limitation to the model.

6. Shear Stress and Strain Field on the planes

Using the relations of solid mechanics, the maximum shear strain on each plane is computable. As mentioned formerly, it is expected that the direction of the maximum shear strain meets the maximum strength and rigidity reduction, and the direction perpendicular to it, which has zero shear strain, not to have strength reduction. The reason why the ellipses of shear strength distribution of the planes in each step of loading are important is explained in section 5. But it should be noticed that non-coaxiality between stresses and strains plays a significant role in anisotropic materials, and should be considered in the shear stress computations of each plane. In the case of calculating shear stress, using Eqs. (15) and (16), the obtained shear stress will all be coaxial with the shear strain of that plane. But considering the anisotropy in the context of material and different rigidity factors in different directions and different planes, and also considering the effect of different paths of strain, the principal axes of stress tensor, computed by Eq. (8), will not necessarily conform to the principal axes of strain tensor. In an anisotropic material, shear component of stress and strain might be non-coaxial. Although the shear stress computed by Eq. (15) is parallel to the shear strain of the plane, for being more compatible to reality, it should be borne in mind that distribution of shear stress on a specific plane is not necessarily coaxial with shear strains either. As distribution of normal stresses around a point is simultaneously influenced by strain distribution and stiffness distribution, shear stresses are not exceptions to this rule either. In previous models, shear stresses of the planes were obtained by the multiplication of maximum shear strain, initial shear elastic modulus and modified rigidity factor of the plane. Hence shear stress vectors of the plane will be co-axial. As mentioned before, the impact of anisotropy and stiffness distribution should be applied to the calculation procedure. For this, the

concepts "*shear stress field*" and "*shear strain field*" are introduced in Ref. [23]. According to the method presented in this Ref., instead of considering only one strain vector on each plane, a field of strains operating on the plane, are considered simultaneously. This way, the effect of no direction on the plane will be missed. The components of this field are also the projection of continuum strain tensor on a plane and in different directions, which are obtained utilizing solid mechanics formulas. In this field, the sizes of strain vectors in different directions vary from zero to the maximum strain of the plane. In each direction, the value of shear stress vector is computed by using Eq. (15 or 16) and in an ordinary way. Same as previous instructions, the ellipse of shear rigidity factors on the planes, in each step of loading, should be updated. In other words, the amount of $RF_T.(1-\omega^0_{Shear}).E^0_T$ in each step should be updated, considering the variations in distribution of rigidity factors. Using solid mechanics formulas and relations, it can be proved that the distribution of strain vectors around a point on a plane, makes a shape like the red circle in Fig. 7. Multiplying strain vectors and scalar values of the modified rigidity factors of each specific direction, the stress vector of that specific direction is obtained. Fig. 7 demonstrates the summary of these operations in a conceptual way.

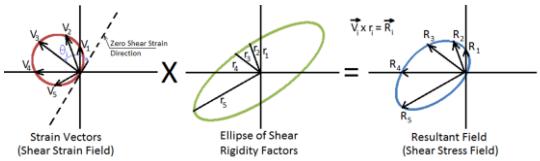

Fig. 7. Computation method of shear stress field due to shear strain field and shear rigidity factors on different planes

Continuous variations in the ellipse of rigidity factors distribution and stress and strain vector fields are conceptually shown in Fig. 8. As can be seen from this figure, by increasing and rotating the direction of strain vectors field (red circle), the ellipse of shear rigidity factors (green ellipse) gets smaller and rotate over time. Shrinkage of the dimensions of the ellipse means deterioration of strength and degradation of stiffness, and its diversion also means variation in the fabric of grains of material. The product of multiplying strain vectors field by the values of the modified rigidity factors creates stress vectors field (blue figure). But in order to compute integration of Eq. (8) and obtain the macroscopic stress of the point, there should be only one stress vector on each plane so that it can participate in calculations. This stress stands for the whole stress vectors of the field on plane, the components of which are computed using the following relations:

$$S_r^1 = \frac{2}{\pi}\int_{\theta=0}^{\theta=\pi} S_\theta.\mathrm{Sin}(\theta)\,d\theta \tag{18}$$

$$S_r^2 = \frac{2}{\pi}\int_{\theta=0}^{\theta=\pi} S_\theta.\mathrm{Cos}(\theta)\,d\theta \tag{19}$$

$$\theta_r = \mathrm{Arctan}(\frac{S_r^2}{S_r^1}) \tag{20}$$

In Eqs. (18) to (20), S_θ is the magnitude of stress vector in direction θ. Also S_r^1, S_r^2 and θ_r are components of representative shear stress vector of the plane and the angle of this representative vector, respectively. Directions θ_r and θ are computed with respect to the direction of zero strain vector on each plane.

Damage parameters and anisotropy parameters of the suggested model, which have been found through the calibration method, for Toyoura sand with 82 percent density, is presented in Ref [23], and the results are shown in table 2.

Table 2. Model parameters for Toyoura sand with relative density of 82% [23]

Damage Parameters				Anisotropy Parameters			
$a_{compressive}$	$b_{compressive}$	a_{shear}	b_{shear}	A_{Nc}	C_{Nc}	A_T	C_T
0.0045	1.0	0.001	1.5	1.0	1.31	1.0	1.38

Other parameters such as elastic modulus and Poisson ratio are computed directly considering the loading test result, and are respectively equal to 110 MPa and 0.28.

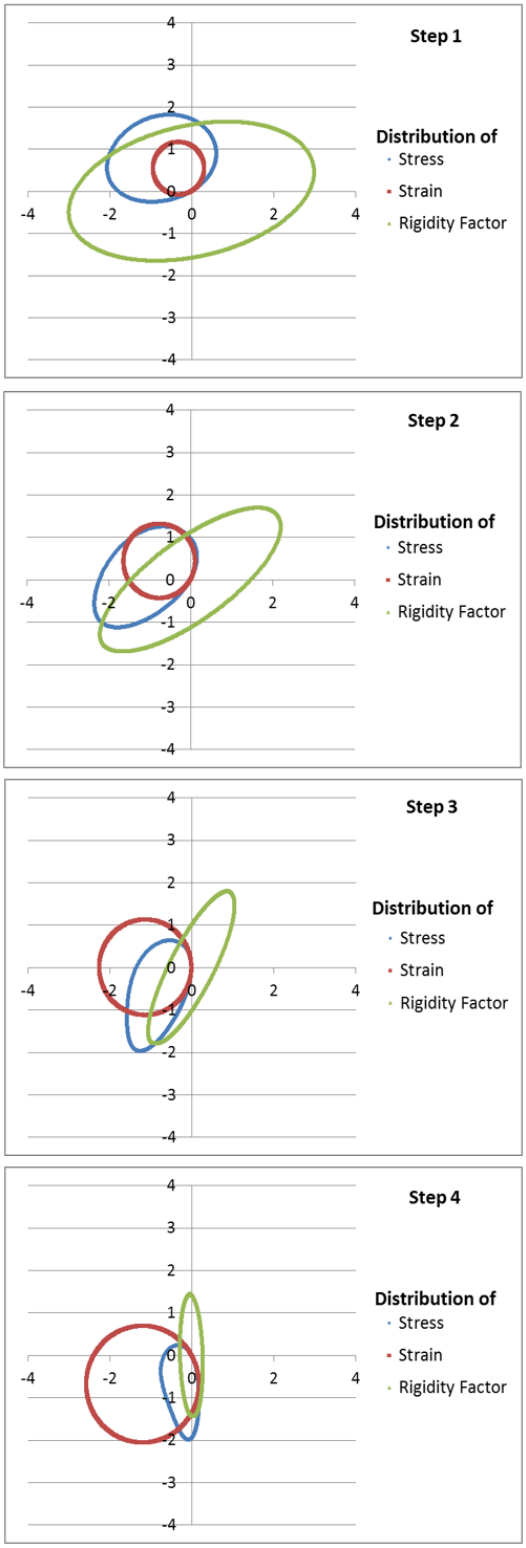

Fig. 8. Successive variation and rotation of shear stress field due to variation of shear strain field and rigidity factor ellipse

7. Adding New Model to the OpenSees program

In order to take advantage from the suggested model in solving more complicated engineering problems, a code is written to introduce the model to the Opensees FEM (finite element method) program. This code is being called and used by the main program, for the application of finite element method successively [36]. Opensees program includes several codes and subroutines which are named "classes". These classes are written and developed over time by the Opensees programming group or other users. The new developed model in this study is called "Ncmm" and is a subset of "nDMaterial" class.

8. Introducing the Properties of the Sample under Study

In order to examine the developed model, the experimental results of a real sample should be compared to the theoretical results obtained from Opensees program. For this purpose, a sample of anisotropic geo-material, like sand or stone, should be considered, so that its characteristics to be experimentally compared with theoretical results. Items such as strength of material, variation in the fabric of the grains and rotation of the principal axes of stress and strain tensor should have been seen in the given experimental study. After searching and reviewing different experimental studies, eventually a laboratory sample was selected. A sample made from standard Toyoura sand, which had been loaded to the extent of creation of shear band. In this laboratory research, issues such as shear-driven volume expansion, fabric variation of the grains and rotation of the strain tensor principle axes have been investigated. In the sample under study, the test was taken as drained (dry) under the plane strain condition. Dimensions of the sample had 180 mm height, 160 mm length and 80 mm width. The specifications of the test apparatus and method of providing the sample under study are explained in detail in Ref. [36]. The sample density is 90%. The principal normal stress σ_1 is applied by the pressure of a thick horizontal plate. Circumferential stress σ_3 is also adjusted through internal negative pressure from inside the sample itself, equal to $49.0\ kN/m^2$. Displacement and deformation of the sample in direction 2 are prevented, and it has no strain in this direction,

i.e., $\varepsilon_2 = 0$. The geometrical details of the sample are illustrated in Fig.9.

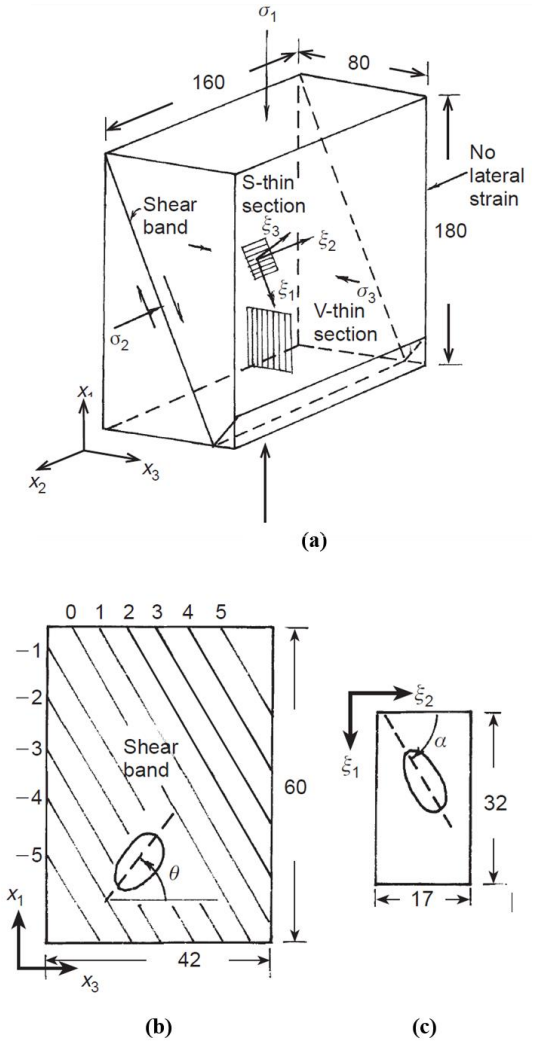

Fig. 9. Compressive test sample of standard Toyoura sand (a) Reference axes (b) V section (b) S section [36]

Thin sections V and S which are seen in Fig. 9(b) and 9(c), are small laminates. They are extracted and separated from the deformed sample at the end of the test to study microscopic variation of fabric of grains. Section V is perpendicular to axis 2, and section S is parallel to the shear band.

For simulating the mentioned sample test in OpenSees program, using finite element method, first of all, the parameters of material should be introduced to the program. The material used in this test, are the same standard Toyoura sand. However, it should be noted that the relative density of material used in this test is different from that of the Ref. [23] test. So the parameters should be cautiously used, and the value of parameters considered for the model should be the result of model calibration for the material with similar density. In the test program which was conducted by Miura et al in Ref. [2] to investigate non-coaxaility of Toyoura sand, density of the sand used at the beginning of the test equals 82%, and then consolidates under confinement pressure 98 kPa. But in the shear band test, being studied in this paper, situation is different. In this test, the relative density of Toyoura sand had initially been 90%, and then consolidates under 49 kPa confinement pressure. So these two tests are different from the viewpoint of density and consolidation pressure. After implementing the computations for both types of sand, it could be shown that the sand with relative density of 82% reaches the relative density of about 90%, upon the isotropic consolidation, under the confinement pressure of 98 KPa. On the other hand, the sand with relative density of 90%, reaches the relative density of about 92.5%, upon the isotropic consolidation under the confinement pressure of 49 kPa. It should be noted that the volumetric elastic modulus is not constant during consolidation, and is variable instead. Considering the above explanations, it is clear that the values of material relative density are close to each other, upon multilateral consolidation, and fortunately a difference of 2.5% is not significant. Therefore, considering that other conditions and characteristics of sand are uniform, use of the parameters of the first test is permitted in the simulation of second test.

9. Sample Meshing

In finite element analysis, the result of analyses is usually different comparing to the element dimensions, even using elements with the same type. This means that the theoretical results of the same sample analysis, with various dimensions of element, are different. Therefore, in each finite element analysis for different problems, first the sensitivity of the simulated sample to the dimensions of elements should be focused on. For this, in this study also, analyses by different dimensions of same type elements have been performed, and the results have been compared with the macro-level experimental results presented in Ref. [36]. In this study, at the first step of sensitivity analysis, in five separate

analyses, the sample with 8-node hexahedral cubic elements, SSPbrick, were meshed uniformly with dimensions of 2, 2.5, 5, 10 and 20 mm. Diagrams of macro-level stress-strain, which are derived from these analyses for the mentioned meshing sizes, are shown in Fig. 10(a). As can be seen from this Fig., the values of the predicted strengths were higher for bigger meshing, and the maximum strength occurs in smaller strains. The reason for this is attributable to the greater effect of applied boundary conditions and the increase in the value of the effect of confinement pressure. According to the conditions of testing apparatus, the bottom supporting conditions below the sample are defined the way that all transitional degree of freedoms of the nodes are restrained in this level. Supporting conditions above the sample are also defined the way that the degrees of freedom of all points are bound together in lateral direction (3). In fact, the adjacent points in the upper jaw of the test apparatus are not able to move independently in lateral direction, and all of them move together and to the same extent, to the lateral direction. Considering the above explanations, it is clear that the support conditions have an important impact, and if the used elements are not of suitable dimensions, their effects on problem solving conditions will be more than necessary, and confinement pressure in the elements will be estimated more than what they really are. This factor eventually leads to unreal prediction and excessive strength.

For more precise study on this subject, volumetric strain variations versus axial strain are compared for analyses with different meshing against the experimental values in Fig. 10(b). It is clear that dilatant volumetric strain is smaller for bigger dimensions of meshing. Since the test is taken under plane strain conditions, the value of $\varepsilon_2 = 0$ and thus the value of volumetric strain will be equal to $\varepsilon_V = \varepsilon_1 + \varepsilon_3$, where the value of ε_1 will always be negative and the value of ε_3 will always be positive. Considering the diagrams in Fig. 10(b), it is clear that the values of ε_V are smaller for the analytical samples with bigger meshing elements. This is indicative of the fact that the impact of support conditions was such that less lateral strain values have been occurred in samples with bigger meshing dimensions.

According to Diagrams 10 (a) and (b), it is clear that the results predicted by the 5 mm element is sufficiently close to the experimental results, and the maximum value of analytical strength is only 5.6% higher than the precise experimental value, which is a satisfying precision. In addition its computational cost is much lower than those of 2 and 2.5 mm.

10. Deformation of Samples with Different Meshing

In this section, deformation of different parts of the analyzed samples is studied using finite elements program Opensees with assistance of the model introduced in previous sections. The cubic sample introduced in this section is studied using meshing dimensions 5, 10 and 20 mm. The obtained analytical results for different values of deformation in different parts are studied.

Figs. 11(a) to 11(c) show the contour of vertical and lateral deformation for meshing with different dimensions. All the figures are related to the axial strain of 3.6 percent of the sample. This strain is related to the post peak loading area where variations of stress versus strain have reached a stable and fairly constant condition.

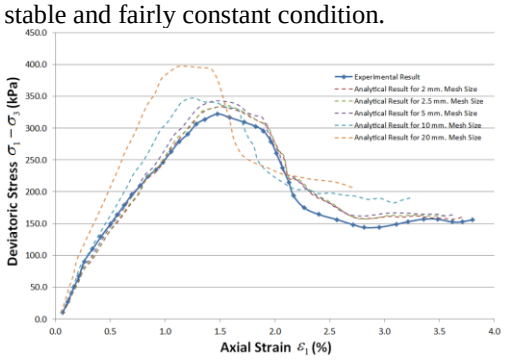

(a)

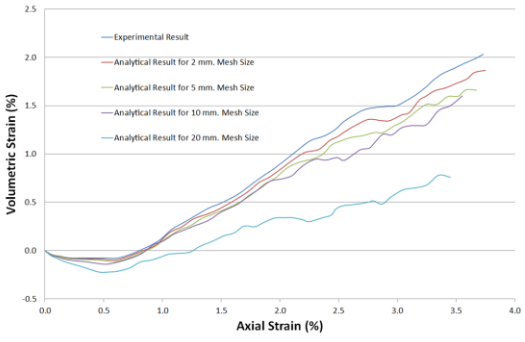

(b)

Fig. 10. Comparison of experimental and analytical results with different meshing of analytical sample (a) Deviatoric Stress vs. Axial strain (b) Volumetric Strain vs. Axial strain

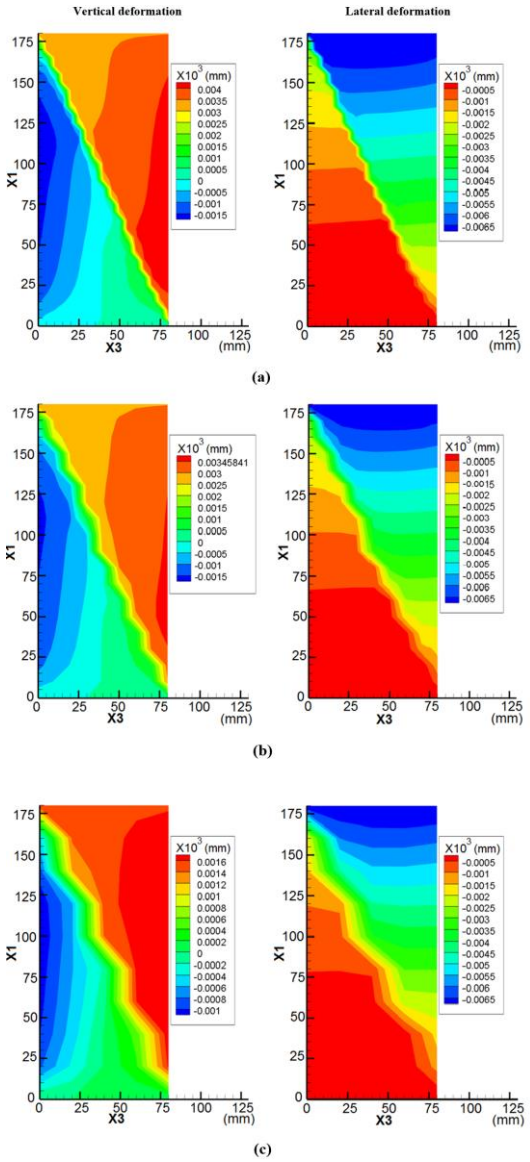

Fig. 11. Deformation contour of the analytical sample with uniform cubic elements with different dimensions (a) 5mm meshing (b) 10mm meshing (c) 20mm meshing

The process of destruction and formation of shear band is clearly seen in these Figures. Also considering these Figures, it is clear that the residual deformation, derived from the former steps of loading, has still remained to some extent, and is visible. For example, before the formation of shear band and sliding of the upper part over the lower part, lateral deformations on the mid parts are more than those at the sample ends which are affected by jaw friction. But by the outset of shear band formation, reduction of the values of macro-level vertical stress and redistribution of strains, some of these deformations reduce and some others remain in the sample, as is visible in the presented contours.

It should be noted that to impose the formation of a one-way shear band, 3 percent of the applied axial displacement is horizontally applied to the nodes adjacent to the upper support in the input file, in each step. Otherwise, the shear band forms in X symmetrical way, and the obtained strength values will be different.

Considering the numbers presented beside the contours, it is clear that the values of axial and lateral deformations are smaller for the samples with larger elements. The reason was previously studied, and it was specified that it is due to the greater impact of lateral constraint of supports and the increase in the confinement pressure of elements. For example, focusing on the contour values of vertical deformations in the lower half of the sample, it is clear that the red area adjacent to the lower support, which is correspondent to the normal deformations of zero or near zero, becomes larger and expands by increasing the size of the element dimension. As the same way, in upper levels, the contours that correspond to less deformation values, expand more as well.

It should be noted that after the formation of shear band in the sample, the upper half, in addition to stress driven deformations, will experience rigid body displacement, as well. This displacement is the result of sliding and movement of the upper half of the shear band on the lower half. According to the inclination of the formed shear band, rigid body displacement of the upper half of the sample exists in both vertical and horizontal directions, thus in studying the displacement of points, this should be considered. This type of rigid body displacement in Fig. 12, which is obtained from the experimental results of the test, is displayed in form of difference in the elevations of the different layers of sample, and has a good conformity with the computational results of Fig. 11(a).

With an overview on the Figs. 11(a) to 11(c), it turns out that the average estimated widths of the shear band, are 4, 8 and 12 mm, respectively. These figures are obtained from measuring the distance between the adjacent points in the direction of the maximum gradient of displacement. The location of these points is selected to be the same experimentally measured locations of Fig. 12. Shear band obtained from the

experimental results are also shown in Fig. 12, and its width is observable in different areas.

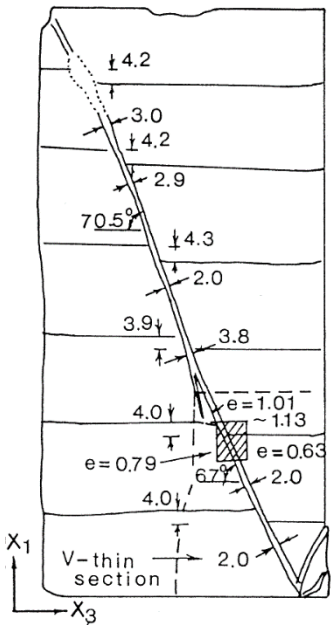

Fig. 12. Experimental results of the shear band width and vertical displacement of the upper half in Toyoura sand test [36]

11. Variations of Damage Factors in Different Sample planes

For more inspection of the performance of the suggested model, the diagrams of damage factors variations are investigated in this section. By increasing the vertical macro-level strain in the sample, normal and shear strains of different planes also change. These changes in the strain of planes lead to variations in damage factors, the diagrams of which are presented in Fig. 13. The case under study in this section is of 5mm meshing. These diagrams are presented for two different elements from two different areas of sample. One point is selected above and another point at the shear band area. Considering the variation of each of the damage functions and their growth speed, type of damage and the plane on which damage begins could be found.

In Fig. 13(a), variation of compressive and shear damage factors for a zone a little above the shear band, is shown. Taking a glance to this figure, it is clear that compressive damage is not very probable above the sample shear band. The maximum probable damage at this point is less than 0.8, which is far enough from completely damaged limit. This value of maximum damage belongs to the plane No. 13 which is horizontal and loading direction of the sample plane is perpendicular to this plane. Of course, its value remains constant upon reaching a maximum value. According to the assumption stated in section (3), with the reduction of strains, damage magnitude remains constant. Following to the plane No. 13, there are planes such as 14, 15, 16 and 17 which are almost close to the horizon, and suffer from a considerable compressive damage. Although planes such as 10, 1 and 3 did not suffer a considerable compressive damage at the beginning of loading, they show a significant growth in compressive damage factor by the outset of shear band formation and principal axes rotation.

Taking a look on Fig. 13(b), it is clear that the element under study has greater values of shear damage in comparison to compressive damage. According to the value of the maximum shear damage factor of 0.9 in planes 9 and 10, it can be said that occurrence of shear damage in these planes is more probable, in comparison to others. From the viewpoint of spatial orientation, these planes are the closest ones to the plane on which shear band occurs. After the mentioned planes, there are also planes 1 to 4 and after them, planes 16 and 17. Of course, by shear band formation and principal axes rotation, shear damage factor in planes No. 16 and 17 overtake other planes, and experience the highest shear damage at the area above the shear band.

At the shear band area also, according to Fig. 13(c and d), shear damage is absolutely undoubted, but at the same time, the sample compressive damage in this area is also considerable. The value of shear damage factor in this area amounts to 0.95, and it can be claimed that complete shear damage is occurred. The maximum value of shear damage at the early stages of loading occurs in planes 9 and 10, and for this, it behaves similar to the upper area of the shear band. But after shear band formation and axes rotation, planes 16 and 17 overtake other planes and record the maximum value of shear damage in the whole sample. The reason for this is that planes 16 and 17 are the closest ones to the shear band, so they have experienced the greatest increase in the value of shear damage. Regarding the compressive component, it can also be seen that at the commencement of loading, plane No. 13 had the highest growth but upon shear band

formation, the damage of planes 14 and 15 has grown fast, and reached about 0.87. This is actually indicative of the fact that the shear band zone not only suffers from shear damage but also compressive strength capacity reduces considerably. Considering the above explanations, and comparing them with experimental observations, it is clear that damage functions can accurately predict the type and degree of the damage. According to the plane in which damage occurs, failure direction can also be found, which was proved to be in good conformity with reality.

12. Variations of Compressive and Shear Rigidity Factors in Different Directions of the Sample

The value of compressive strength in different directions decreases by an increase in loading. To clarify the matter, compressive rigidity factors are presented in Figs. 14 and 15. These figures show the variations of the compressive rigidity factors for the lower part of the shear band and the shear band itself, respectively. In these figures the ellipsoid of initial compressive rigidity factors are shown in red dashed diagram and rigidity factors distribution in following increments are also shown in blue diagram.

It is obvious that in Fig. 14, which is related to the lower part of the shear band, distribution of compressive rigidity factors involves in declination and reduction, but not much rotation occurs on its main axes. Strength reduction is also mostly related to the horizontal, or near horizontal, planes which are perpendicular to the loading direction.

On the contrary, paying attention to Fig, 15, which is related to the shear band area itself, it can be seen that in addition to strength reduction due to loading, rotation also exists in the main axes of strength distribution. In this figure, considering the process of changes in the blue diagram, it can be seen that right upon the outset of shear band formation, the principal axes of diagram considerably start rotating as well.

Comparing the two Figs. 14 and 15, it is clear that strength reduction is higher around the shear band and rotation of axes of strength distribution diagram has considerably occurred in this area and is of great importance. This strength diagram rotation itself is resulted from fabric variation on which comprehensive explanations have been presented formerly.

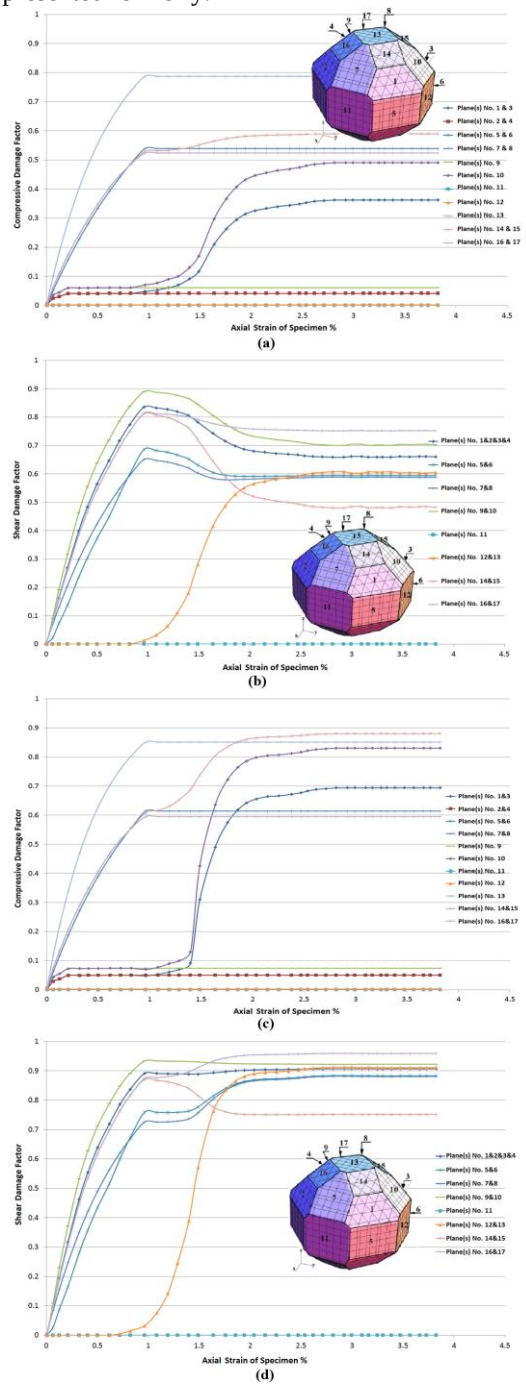

Fig. 13. Damage factors variations vs. axial strain increment of the analytical sample (a) Compressive damage above the shear band (b) Shear damage above the shear band (c) Compressive damage at the shear band area (d) Shear damage at the shear band area

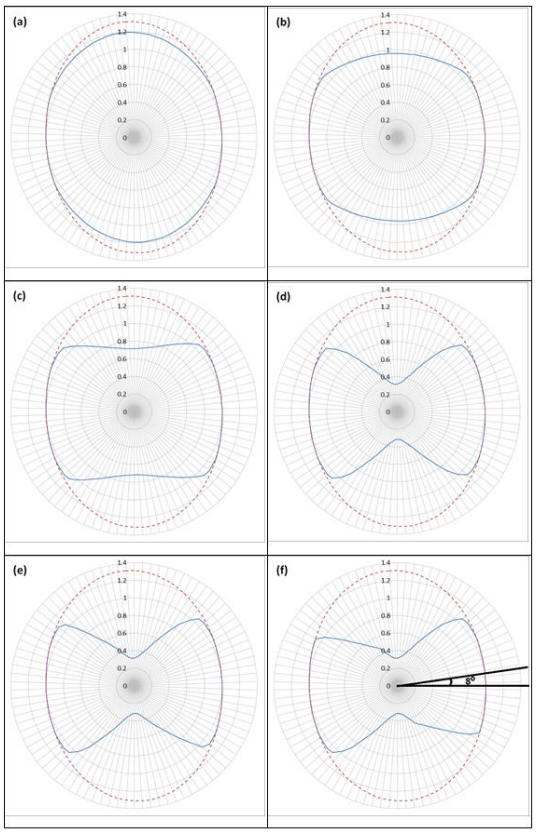

Fig. 14. Variation of compressive damage factors of analytical sample during loading (below shear band)

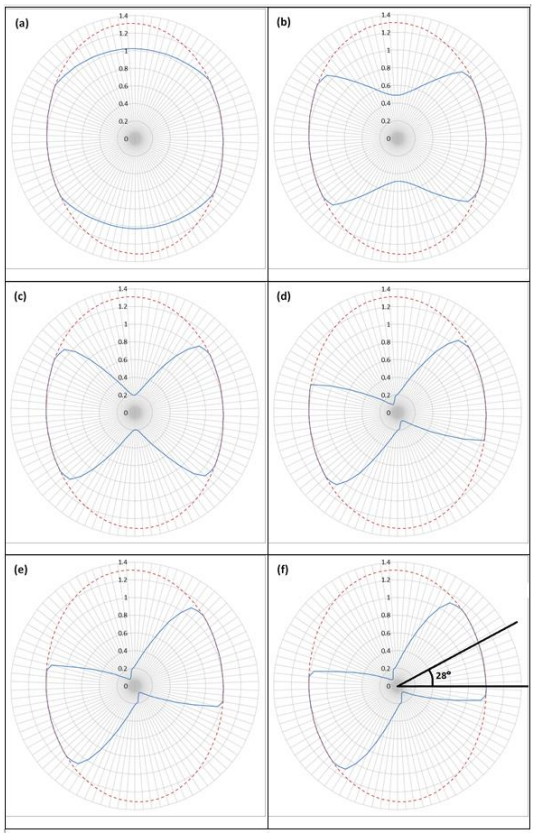

Fig. 15. Variation of compressive damage factors of analytical sample during loading (mid area of shear band)

Shear ellipses of the plane rigidity factors also change during loading. As mentioned before, these ellipses at the start of loading were the result of the crossing of shear rigidity factor ellipsoids and different planes, and their shape and angle change during loading. To this end, at the shear band area, which is subject to the most rotation of the strain tensor principal axes, the consecutive variations of the ellipse of shear rigidity factors for planes 7, 10 and 17, are displayed in Figs. 16(a) to 16(c).

According to Figs. 16(a) to 16(c), it is seen that, depending on the positioning of plane, the ellipses of rigidity factors may show different behaviors. Some of these ellipses only face strength declination, and rotation does not occur on their axes, whereas in some other planes, in addition to strength reduction, rotation may occur on their axes. Eventually by using these ellipses on different planes, fabric and arrangement of grains and their variations could be found.

13. Variation in Fabric of Grains in Different Planes of Sample

In the previous sections it was stated that the loading process leads to fabric variation. It was also explained that considering the strength or rigidity which are the effects of material fabric, the grains orientation in each step of loading can, to a great extent, be specified. Therefore, in this section, comparing the measured empirical and analytical results, it is tried to display the ability of the suggested model in this regard.

Position and orientation of planes V and S are described in section (8) and Fig 9(b) and (c). In this figure, the grains rotation angles on planes V and S, which are named θ and α, respectively, are shown as well. These angles measure and show the diversion and rotation of the grains longest dimension during loading. Planes parallel to V in Fig. 9(b) divides the sample into some areas, where the shear band is located in area (-1,0). Area (-2,-1) is also located below the shear

band.

Distribution of the grains angle variation and their frequency ratio for plane V are shown, around the shear band and below it in Ref. [36]. According to the data given in this Ref., the average angle variation of the grains, which is empirically measured, is about 28.4º around the shear band and 7.9 º below the shear band. Formerly in section (5) in explaining induced anisotropy, it was explained how the grains and sand particles attach each other and make load transferring columns. According to empirical and laboratory observations, sand particles in these columns lean together from the bigger side, in order to provide a larger surface for load transferring. On the other hand, the most reduction of compressive rigidity and strength in the sample will be in the direction of columns formation. Therefore, according to the distribution of rigidity factors observed around a point, the direction of columns will be the very direction with the maximum rigidity reduction, and the direction perpendicular to it also shows the long dimension of the sand particles. Focusing on Figs. 14(f) and 15(f), which respectively relate to the rigidity factors distribution of areas below and around the shear band, the average angle variation of the principal axes of Figs. is 28º and 8 º. This rotation of axes of the diagram of rigidity factors distribution, shows the grains rotation, which well conforms to the empirical value.

Frequency distribution of angle variation of grains on plane S is also shown in Ref. [36]. According to the given information, the average value of the rotation of grains, which is empirically measured, equals 77º. Among the 17 planes around the polyhedron, the closest plane to the shear band is plane No. 7 which in fact is not completely parallel to the shear band plane. But to study the issue, the analytical results of that plane, inevitably is used and presented in Fig. 16(a). According to this Fig., it is observed that the principal axes of the ellipse of shear rigidity factors distribution on this plane rotates for about 52º. Since the material shear rigidity factor is affected by its grain's orientation, this angle variation of the axes of shear rigidity factors distribution exactly reflects the value of sand particles rotation. Therefore, the "cause" could be found via "effect". This value is 25º different from reality. There are some reasons to justify the discrepancy. The value of 77º is the highest frequency of distribution of grains longest axis orientation and of course the average value is much lower than this according to the reference. The other reason may be attributable to the thickness of the shear band and the location of which the angles of grains are measured and potentially are a little different from the element under study. Finally, the most important reason of this difference is the non-conformity of the shear band plane and plane No. 7, the analytical results of which are investigated. But the rotation of sand particle itself, and its orientation is correctly predicted in a conceptual manner.

14. Summary and Conclusion

1- The ellipsoids of shear and normal rigidity factors define a uniform and comprehensive mathematical rule around a material point, by which strength and rigidity factors of the material at each step of loading in any direction could be predicted and followed. Since the rigidity and strength of material depend on the texture and fabrication of sand particles, the occurred variations in the ellipsoids are indicative of the variations of the fabric and arrangement of sand particles.

Applying the defined laws and damage factors values, it will be possible to compute the diversion of ellipses and ellipsoids. By using the damage factor values of each plane, direction and type of failure are also predictable, and eventually the type of failure and destruction of the sample will be predicted and interpreted.

2- Non-coaxiality of stress and strain is also an inseparable component of the anisotropic material models. In this type of materials, considering the empirical and laboratory evidences, stress and strain vectors are not coaxial, and to achieve accurate computations on the behavior of material, the given model should be able to predict and compute it. According to the increase in anisotropy or inelasticity of material, the importance of this issue increases. Predicting this important behavioral characteristic of anisotropic material have become possible, using methods and techniques in the suggested model.

3- After developing the given model, an operational program, in form of finite elements method for solving bigger problems, has been written, and introduced to Opensees as a new behavioral model. This code, as an operational program, provides the finite element program with the new model, so that it can use this model in solving bigger problems. Finally, the program

analysis results were compared to the empirical results. Comparing the results proved the operational accuracy of the model, and it was found that the model has the competence to be applied to bigger problems.

4- In real-world scenarios, we mostly deal with anisotropic materials. This research reveals that studying the behavior of anisotropic materials under the influence of rotational stresses is significantly different from the behavior of isotropic materials. In this case, stress and strain axes are not aligned with each other, leading to changes in the structure and texture of materials over time. Studying behavior models for anisotropic materials under variable stresses is of great importance in drilling industries, especially in the oil and gas upstream sector, which is cost-intensive. Inadequate and insufficient studies in this regard can result in operational failures.

15. References

[1] Ghasemzade H. and SanayePasand M. “Thermo-Hydrodynamic modelling of hydrocarbon reservoirs” Journal of Petroleum Geomechanics, 2019 Jun., pp. 60-80. (In Persian)

[2] Miura, K., Miura, S. and Toki, S., (1986), "Deformation behavior of anisotropic dense sand under principal stress axes rotation" Soils and Foundations, (1986) Vol.26-1, pp. 36-52.

[3] Yang Y, Yu HS. Application of a non-coaxial soil model in shallow foundations. Geomechanics and Geoengineering: An International Journal. 2006 Aug 31;1(2):139-50.

[4] Gräbe PJ, Clayton CR. Effects of principal stress rotation on permanent deformation in rail track foundations. Journal of Geotechnical and Geoenvironmental Engineering. 2009 Apr;135(4):555-65.

[5] Yang L. Experimental study of soil anisotropy using hollow cylinder testing (Doctoral dissertation, University of Nottingham).

[6] Bažant ZP. Comment on orthotropic models for concrete and geomaterials. Journal of Engineering Mechanics. 1983 Jun;109(3):849-65.

[7] Bažant, Z. and Oh, B. (1985). "Microplane Model for Progressive Fracture of Concrete and Rock" J. Eng. Mech., (1985) Vol. 111-4, pp. 559-582.

[8] Borja RI, Sama KM, Sanz PF. On the numerical integration of three-invariant elastoplastic constitutive models. Computer methods in applied mechanics and engineering. 2003 Feb 28;192(9-10):1227-58.

[9] Li, X. and Dafalias, Y. (2002). "Constitutive Modeling of Inherently Anisotropic Sand Behavior" J. Geotech. Geoenviron. Eng., (2002), Vol. 128-10, pp. 868-880.

[10] Gao ZW, Zhao JD, Yao YP. (2010). "A generalized anisotropic failure criterion for geomaterials" Int J Solids Struct, (2010), Vol. 47-(22-23), pp. 3166–3185.

[11] Cai Y, Yu HS, Wanatowski D, Li X. Noncoaxial behavior of sand under various stress paths. Journal of Geotechnical and Geoenvironmental Engineering. 2012 Oct 10;139(8):1381-95.

[12] Tong ZX, Zhang JM, Yu YL, Zhang G. Drained deformation behavior of anisotropic sands during cyclic rotation of principal stress axes. Journal of Geotechnical and Geoenvironmental Engineering. 2010 Apr 30;136(11):1509-18.

[13] ISHIHARA K, Towhata I. Sand response to cyclic rotation of principal stress directions as induced by wave loads. Soils and foundations. 1983 Dec 15;23(4):11-26.

[14] Nakata Y, Hyodo M, Murata H, Yasufuku N. Flow deformation of sands subjected to principal stress rotation. Soils and Foundations. 1998 Jun 15;38(2):115-28.

[15] Zhou J, Yan J, Xu C, Gong X. Influence of intermediate principal stress on undrained behavior of intact clay under pure principal stress rotation. Math Probl Eng 2013;25(2013):1–10.

[16] Zhou J, Yan JJ, Liu ZY, Gong XN. Undrained anisotropy and non-coaxial behavior of clayey soil under principal stress rotation. Journal of Zhejiang University Science A. 2014 Apr 1;15(4):241-54.

[17] Yan JJ, Zhou J, Gong XN, Cao Y. Undrained response of reconstituted clay to cyclic pure principal stress rotation. Journal of Central South University. 2015 Jan 1;22(1):280-9.

[18] Bažant P, Oh BH. Efficient numerical integration on the surface of a sphere. ZAMM Journal of Applied Mathematics and Mechanics/Zeitschrift für Angewandte Mathematik und Mechanik. 1986 Jan 1;66(1):37-49.

[19] Christoffersen J, Mehrabadi MM, Nemat-Nasser S. A micromechanical description of granular material behavior. Journal of applied mechanics. 1981 Jun 1;48(2):339-44.

[20] Oda M, Konishi J, Nemat-Nasser S. Some experimentally based fundamental results on the mechanical behaviour of granular materials. Geotechnique. 1980 Dec;30(4):479-95.

[21] Taheri E, Sadrnejad SA. Prediction of internal mechanism of soil upon multiplane framework. In:

Proceedings of International Conference on Geotechnical Engineering and Soil Mechanics. Tehran, Iran; 2010: Paper No. & Code: 029.

[22] Ghadrdan M, Sadrnejad SA, Shaghaghi T. Numerical evaluation of geomaterials behavior upon multiplane damage model. Computers and Geotechnics. 2015 Jul 1;68:1-7.

[23] Sadrnejad SA, Shakeri S. Multi-laminate non-coaxial modelling of anisotropic sand behavior through damage formulation. Computers and Geotechnics. 2017 Aug 1;88:18-31.

[24] Bažant ZP, Caner FC, Carol I, Adley MD, Akers SA. Microplane model M4 for concrete. I: Formulation with work-conjugate deviatoric stress. Journal of Engineering Mechanics. 2000 Sep;126(9):944-53.

[25] Carol I, Bažant ZP. Damage and plasticity in micro-plane theory. Int J Solids Struct.. 1997;34(29):3807–3835.

[26] Schädlich B, Schweiger HF. Anisotropic small strain stiffness within the multilaminate framework. In7th European Conference on Numerical Methods in Geotechnical Engineering 2010 May 25. Balkema.

[27] Choo J, Jung YH, Cho W, Chung CK. Effect of pre-shear stress path on nonlinear shear stiffness degradation of cohesive soils. Geotechnical Testing Journal. 2013 Jan 24;36(2):198-205.

[28] Likitlersuang S, Teachavorasinskun S, Surarak C, Oh E, Balasubramaniam A. Small strain stiffness and stiffness degradation curve of Bangkok clays. Soils and Foundations. 2013 Aug 1;53(4):498-509.

[29] Carol I, Bažant ZP, Prat PC. Geometric damage tensor based on microplane model. Journal of engineering mechanics. 1991 Oct;117(10):2429-48.

[30] Sadrnejad SA, Shakeri S. Fabric assessment of damaged anisotropic geo-materials using the multi-laminate model. International Journal of Rock Mechanics and Mining Sciences. 2017 Jan 1;91:90-103.

[31] Kutter BL, Chen YR, Shen CK. Triaxial and Torsional Shear Test Result for Sand, California USA: Dept. of Civil Engineering, University of California at Davis; 1994.

[32] Tong ZX, Zhang JM, Yu YL, Zhang G. Drained deformation behavior of anisotropic sands during cyclic rotation of principal stress axes. Journal of Geotechnical and Geoenvironmental Engineering. 2010 Apr 30;136(11):1509-18.

[33] Oda M, Konishi J, Nemat-Nasser S. Experimental micromechanical evaluation of strength of granular materials: effects of particle rolling. Mechanics of materials. 1982 Dec 1;1(4):269-83.

[34] Oda M, Nemat-Nasser S, Konishi J. Stress-induced anisotropy in granular masses. Soils and foundations. 1985 Sep 15;25(3):85-97.

[35] OPENSEES Team (2012, Feb 16). Adding your own code. Retrieved 2018, Apr. 15, from http://opensees.berkeley.edu/wiki/index.php/Adding_your_own_Code

[36] Oda M, Kazama H. Microstructure of shear bands and its relation to the mechanisms of dilatancy and failure of dense granular soils. Geotechnique. 1998 Aug;48(4):465-81.